https://doi.org/10.1007/s00161-018-0726-7

D. George · R. Allena · Y. Rémond

Integrating molecular and cellular kinetics into a coupled continuum mechanobiological stimulus for bone reconstruction

Abstract The development of multiphysics numerical models to predict bone reconstruction is a very challenging task as it is a complex phenomenon where many biological, chemical and mechanical processes occur at different lengths and timescales. We present here a mechanobiological theoretical numerical model accounting for both the mechanical and biological environments to predict the bone reconstruction process through the use of a global stimulus integrating the contributions of applied external mechanical loads, cellular activities and cellular nutriments such as oxygen and glucose supply. The bone density evolution will hence depend on the overall stimulus and evolve accordingly to the intensities of each of its individual constituents. We show their specific influences and couplings on a simple two-dimensional geometry and confirm that, although the mechanics plays a crucial role in the bone reconstruction process, it is still highly dependent on the occurring biological events and will evolve accordingly.

Keywords Bone reconstruction · Multiphysical stimulus · Oxygen · Glucose · Cell motility

1 Introduction

The development of predictive models for continuous bone remodelling [1] or bone reconstruction has been going on for a very long time since the early works of Wolff [2]. To be efficient, these models require the use of appropriate theories to account for the specific mechanophysiological phenomena occurring at the microstructural scale. Many works [3–23] have tried to reach this objective, sometimes developing sophisticated theoretical models, but without being able to completely integrate all physiological aspects. Recently, new theoretical and numerical studies [24–30] have appeared to bridge this gap. Nonetheless, many difficulties remain in the understanding of the mechanotransduction processes [31,32] driving this evolution, including healing stages such as vascular growth and nutrient supply [33,34].

The bone density kinetics is often predicted using theoretical models based on a mechanobiological stimulus integrating only the strain energy density developed inside the material through externally applied mechanical loads [7,10,19]. However, if one wanted to approach a good prediction of bone density evolution (being reconstruction or remodelling), other complementary sources, being involved in the process influencing the defined mechanobiological stimulus, such as biological, neurological, electrical, and others, should be integrated. It is of course not possible nowadays to include all these effects as most of them are largely not precisely understood,

D. George (✉) · Y. Rémond
ICUBE, CNRS, University of Strasbourg, 2 Rue Boussingault, 67000 Strasbourg, France
E-mail: george@unistra.fr

R. Allena
Arts et Métiers ParisTech, LBM/Institut de Biomécanique Humaine Georges Charpak, 151 bd de l'Hôpital, 75013 Paris, France

nor quantified experimentally. Hence, in the current work, it was decided to focus specifically on the main biological sources driving the bone density evolution being the cells and their viability in time. Experimental studies have already shown that oxygen and glucose have an important effect [35–39] showing poor cells survival after implantation with a shortage of glucose. This coupling seems to be a good first choice in order to highlight some of the existing links in bone remodelling between the mechanics (applied forces) and the biology (cells activity and viability).

An example of such mechanobiological couplings is the applied mechanical forces [40] for orthodontic tooth treatments leading to an alteration of cell differentiation due to oxygen concentration variation by the periodontal ligament being partially strained. The supply chain of nutriments and oxygen is modified and can then be used to predict cell recruitment, proliferation and migration, leading to the bone remodelling process. These effects can be triggered by genetic and/or epigenetic factors that impact the overall response of the system and should be implemented within a thermodynamically consistent model [41] and using appropriate homogenization procedures [42]. In addition, the biology requires adequate experimental quantifications such as the bone resorption kinetics, which are four times larger than bone reconstruction's [43], and specific multiscale theoretical approaches [44–46].

We present here a continuous numerical model to predict the bone density kinetics as a function of the coupled mechanical and proposed biological sources, their corresponding constitutive laws, their mutual interactions, and the associated kinetics of each single process. The external sources used here to calculate the global stimulus triggering bone density evolution are : (i) the mechanical energy developed through the applied external forces and sustained by the bone cells, (ii) the concentration of nutriments (we choose here to integrate only oxygen and glucose as the most important factors for cell survival), and (iii) the cell survival and activity triggered by specific levels of oxygen and glucose and dependent on the applied mechanical strain. Although many other biological factors may influence the bone density evolution, as without cells no density change can occur, we hypothesize that these will be the primary factors to lead the mechanobiological couplings.

Two cellular phenotypes are considered here: the osteoclasts, responsible for bone resorption, and the osteoblasts, responsible for bone formation. The cells recruiting, migration and differentiation are described via two diffusion equations [47–49] and will impact directly the bone density kinetics through the calculation of synthesis and resorption rates, respectively as a function of the positiveness of the defined global mechanobiological stimulus [50].

2 Model development

2.1 Theory

In the case of everyday life conditions, the bone is in a state of mechanobiological equilibrium (under gravity) in the so-called lazy zone where little remodelling occurs. However, when additional external load is applied, the system is perturbed and goes out of the "lazy zone". The modified load conditions create a coupled mechanobiological signal that will activate bone remodelling/reconstruction. We define this signal [45] by introducing a Lagrangian configuration $B_L \subset \mathbb{R}^3$ (8, 9, 17), and a suitably regular kinematical field $\chi(\boldsymbol{X}, t)$ that associates with any material point $\boldsymbol{X} \in B_L$ its average placement $\chi(\boldsymbol{X}, t)$ at time t. The kinematics of the system is defined by the Lagrangian density $\rho_b(\boldsymbol{X}, t)$ representing the density of natural bone. The image of the function χ gives at any time t, the current shape of the body being the Eulerian configuration. We also introduce the displacement field $u(\boldsymbol{X}, t) = \chi(\boldsymbol{X}, t) - \boldsymbol{X}$, the tensor $F = \nabla\chi(\boldsymbol{X}, t)$, and the Green–Lagrange deformation tensor $G = \left(F^T.F - I\right)/2$ that can be identified linearized as $\boldsymbol{\varepsilon}$ in small perturbations.

The global stimulus variation ΔS [50] is expressed in the Lagrangian configuration B_L in the form:

$$\Delta S(\boldsymbol{X}, t) = S(\boldsymbol{X}, t) - S_0(\boldsymbol{X}, t) = \prod_{i=1}^{n} \alpha_i \, \Delta S_i(\boldsymbol{X}, t) \,. \tag{1}$$

where $S(\boldsymbol{X}, t)$ is a scalar quantity measuring the activation signal collected at $(\boldsymbol{X}, t)$ by the actor cells, and $S_0(\boldsymbol{X}, t)$ being an activation threshold. t is the time, n is the total number of external sources ΔS_i (i.e. mechanical, biological (cellular, nutrients, …), electrical, …) involved in the process and α_i are their weighting coefficients, triggered by genetic and/or epigenetic factors, allowing to simultaneously control their impact on the overall response of the system as well as their interactions. The α_i set of parameters represent both the quantitative influence of each of the external sources ΔS_i with regards to each other (respective individual ratios), and their quantitative effects on the global stimulus variation ΔS. Hence, they can be patient dependent

quantified as a function of each individual body response, and support biology-only or mechanically only effects on the tissue evolution kinetics. Also, the global stimulus ΔS imposes a variation moving from an initial configuration defined in the state of mechanobiological equilibrium (such as a sitting or standing position) at a given stimulus S_0 being also a contribution of each of the individual mechanical and biological effects.

In the current work, we consider the following external sources: (i) ΔS_{mech} that includes the applied mechanical load through the mechanical energy developed within the system to trigger the biological actions, (ii) ΔS_{ob} and ΔS_{oc} that correspond to the osteoblasts and osteoclasts recruiting and migration and, (iii) ΔS_{O_2} and ΔS_{CHO} that coincide with oxygen and glucose supply necessary for cell survival and work contribution.

(i) The mechanical stimulus $\alpha_{\text{mech}}\Delta S_{\text{mech}}$ is expressed through the "standard" definition of the mechanical strain energy and accounts for the applied mechanical forces sustained by bone cells. It is defined in the Lagrangian configuration with:

$$\alpha_{\text{mech}}\Delta S_{\text{mech}}\left(\boldsymbol{X}, t\right) = \alpha_{\text{mech}} \int_{\Omega_0} f\left[U\left(\boldsymbol{X_0}, t\right)\right] \mathrm{d}\left(\boldsymbol{X_0}, t\right) \exp\left(-D_{\text{mech}} || \chi\left(\boldsymbol{X}\right) - \chi\left(\boldsymbol{X}_0\right) ||\right) \mathrm{d}\boldsymbol{X}_0 \tag{2}$$

with Ω the domain of interest, α_{mech} a weighting coefficient, D_{mech} a characteristic distance accounting for the dependent size effect of the source. $f\left[U\left(\boldsymbol{X_0}, t\right)\right]$ is a function of the strain energy density (that may for example depend on the positiveness of the applied mechanical forces), and d being a function of the bone mass density expressed as $d\left(\boldsymbol{X_0}, t\right) = \eta \frac{\rho_b}{\rho_{\max}}$ with $\eta \in [0, 1]$, and $\rho_{\max}$ the maximum of the Lagrangian bone density, being the density of compact bone (corresponding to minimum porosity). $\boldsymbol{\Omega_0}$ is the Lagrangian configuration of the domain.

(ii) The molecular stimuli $\alpha_{\text{O2}}\Delta S_{\text{O2}}$ and $\alpha_{\text{CHO}}\Delta S_{\text{CHO}}$ are defined with the relation:

$$\alpha_{\text{mol}}\Delta S_{\text{mol}}\left(\boldsymbol{X}, t\right) = \alpha_{\text{mol}} \int_{\Omega_0} f\left(c_{\text{mol}}\right) \exp\left(-D_{\text{mol}} || \chi\left(\boldsymbol{X}\right) - \chi\left(\boldsymbol{X}_0\right) ||\right) \mathrm{d}\boldsymbol{X}_0 \tag{3}$$

where the indice mol can either take the value O2 or CHO. D_{mol} being characteristic distances of molecular activation thresholds. α_{mol} are the weighting coefficients for the functions $f\left(c_{\text{mol}}\right)$ of the oxygen and glucose concentrations (c_{O2},c_{CHO}), respectively, and satisfying the two following partial differential equations (PDEs) as a function of the hydrostatic pressure as follows

$$\boldsymbol{D}_{\text{O2}} \frac{\partial c_{\text{O2}}}{\partial t} = 0 \tag{4}$$

and

$$\boldsymbol{D}_{\text{CHO}} \frac{\partial c_{\text{CHO}}}{\partial t} = 0 \tag{5}$$

where :

$$\boldsymbol{D}_{\text{O2}} = \boldsymbol{D}_{\text{CHO}} = Tr\left(\varepsilon\right) + \phi\left(\varepsilon_I \boldsymbol{\theta_I} \otimes \boldsymbol{\theta_I} + \varepsilon_{II} \boldsymbol{\theta_{II}} \otimes \boldsymbol{\theta_{II}}\right) \tag{6}$$

with Tr the trace of a tensor, ϕ a scalar, ε_I and ε_{II} and $\boldsymbol{\theta_I}$ and $\boldsymbol{\theta_{II}}$ the principal strains and directions and $\otimes$ the tensorial product. The cell survival being directly dependent on each of the glucose and oxygen concentration (i.e. cell apoptosis with no nutriment supply), we choose here to multiply the two nutriment stimuli (it will separate the function $f\left(c_{\text{mol}}\right)$ to two stimuli with the product $c_{\text{O2}} * c_{\text{CHO}}$) to be in accordance with this phenomenon. As the cell apoptosis is not integrated in the current work, nutriment supplies were taken by hypothesis as nonzero (if zero then no stimulus is developed).

(iii) The cellular stimuli ΔS_{ob} and ΔS_{oc} are defined by the osteoblasts and osteoclasts activity and triggered by specific levels of oxygen and glucose concentration together with the intensity of the mechanical force applied. They are given by the relation:

$$\alpha_{\text{cell}}\Delta S_{\text{cell}}\left(\boldsymbol{X}, t\right) = \alpha_{\text{cell}} \int_{\Omega_0} f\left(c_{\text{cell}}\right) \exp\left(-D_{\text{cell}} || \chi\left(\boldsymbol{X}\right) - \chi\left(\boldsymbol{X}_0\right) ||\right) d\boldsymbol{X}_0 \tag{7}$$

where the indice cell can either take the value ob (for osteoblast) or oc (for osteoclast). D_{cell} being characteristic distances of the osteoblasts and osteoclasts activation thresholds. α_{cell} are the weighting coefficients for the

functions $f\ (c_{\text{cell}})$ of osteoblasts and osteoclasts concentrations $(c_{\text{ob}}, c_{\text{oc}})$ respectively evolving with respect to time via two diffusion–reaction equations [47,49] as :

$$\frac{\partial c_{\text{ob}}}{\partial t} = (1-\rho_{\text{b}})\left\{\text{div}\boldsymbol{D}_{\text{ob}}\boldsymbol{\nabla} c_{\text{ob}} + \left[k_{\text{ob}} c_{\text{ob}} + \beta_{\text{oc}} Tr\left(\varepsilon\right) c_{\text{oc}}\right]\right\} \tag{8}$$

$$\frac{\partial c_{\text{oc}}}{\partial t} = (1-\rho_{\text{b}})\left\{\text{div}\boldsymbol{D}_{\text{oc}}\boldsymbol{\nabla} c_{\text{oc}} + \left[k_{\text{oc}} - \beta_{\text{oc}} Tr\left(\varepsilon\right)\right] c_{\text{oc}}\right\} \tag{9}$$

where div and $\boldsymbol{\nabla}$ are the divergence and gradient operators, the diffusion tensors $\boldsymbol{D}_{\text{ob}}$ and $\boldsymbol{D}_{\text{oc}}$ are defined as in Eq. (6), k_{ob} and k_{oc} are the osteoblasts and osteoclasts proliferation rates, respectively, and β_{ob} and β_{oc}, their corresponding differentiation rates. Similar observation as above can be made for the cellular stimuli. Without the presence of the adequate cells in the structure, there cannot be any bone reconstruction nor degradation. Hence the cellular stimulus should be defined in a product form for the function $f\ (c_{\text{cell}})$. However, to simplify the present analysis, we supposed only a differentiation of osteoclasts into osteoblasts and no other transformation. Hence, as the concentrations are also supposed to be nonzero, it is possible to define the $f\ (c_{\text{cell}})$ function with only a simple summation with $c_{\text{ob}} - c_{\text{oc}}$ to obtain the corresponding cellular concentration and cellular stimulus.

For the above PDEs, a zero flux boundary condition is applied on the external free surfaces as it is supposed that there is no exchange with the outer system.

Finally, the variation of bone density ρ_b is described by a first order ordinary differential equation (ODE) with respect to time given by :

$$\frac{\partial \rho_{\text{b}}}{\partial \text{t}} = \mathcal{A}_{\text{b}}\left(\rho_{\text{b}}\right)\left[s_{\text{b}}\left(\Delta S_{+}\right) + r_{\text{b}}\left(\Delta S_{-}\right)\right] \tag{10}$$

where r_b and s_b are the rates for bone resorption and synthesis respectively, depending on the positiveness of the global stimulus ΔS. $\mathcal{A}_b$ is a function of the bone porosity controlling the intensity of the bone remodelling process. With 0% or 100% bone porosity, no cells can be activated (full void or full bone). Hence, maximum cell activation will be somewhere in between. We hypothesize that the maximum will be at 50% and the function $\mathcal{A}_b$ describes this nonlinear continuous evolution through these three points.

It reads $\mathcal{A}_b = k\frac{\rho_b}{\rho_{\max}}\left(1 - \frac{\rho_b}{\rho_{\max}}\right)$ with k (equals 1 by hypothesis) being a suitable parameter that needs to be defined experimentally.

Bone microstructure is highly heterogeneous at local scale; some previous works highlighted the influences of microfluidic flaw on the cell biological response to trigger bone reconstruction [51,52]. Although these effects are important, particularly for the mechanotransduction processes at the interphase, it remains difficult to integrate them at a more macroscopic scale without a proper homogenization scheme. The mechanotransduction process was then simplified to be integrated directly within cell sensitivity to the applied mechanical load at the macroscopic scale. This load is supposedly constant at any given time t of the analysis and transient in time accounting for the effect of local fluid flow being integrated as hypothesis in the link between cell activation and migration processes.

As the proposed model is developed at a macroscopic scale, we define a minimum size representative volume element in which an average bone density can be defined, typically of the millimetre size on a bone CT scan. This will enable to link a locally calculated homogeneous bone density with its corresponding grey scale density of the medical image technique. In addition, as the bone deformation remains small under a typical body weight mechanical load, only a linear elastic behaviour is sufficient. Hence, we consider here the bone as an isotropic linear elastic material whose Young modulus E_b is given by $E_b = E_{b0}\rho_b^3$ [53–55], where $E_{b0} = 20$ GPa is the initial Young modulus of cortical bone and υ_b its corresponding Poisson coefficient equal 0.3 (56).

The global static equilibrium of the system is expressed with the usual equation $Div\,\boldsymbol{\sigma} + \boldsymbol{f_v} = \boldsymbol{0}$, with $\boldsymbol{\sigma}$ and $\boldsymbol{f_v}$ the Cauchy stress and the body forces, respectively.

The theoretical model was implemented using the finite element (FE) code COMSOL Multiphysics® to predict the bone kinetics reconstruction.

2.2 Application

We focus our application on a bone reconstruction problem being a critical size default (typically of the order of several centimetres for a bone fracture or surgery) that needs to be rebuilt. A critical default along the

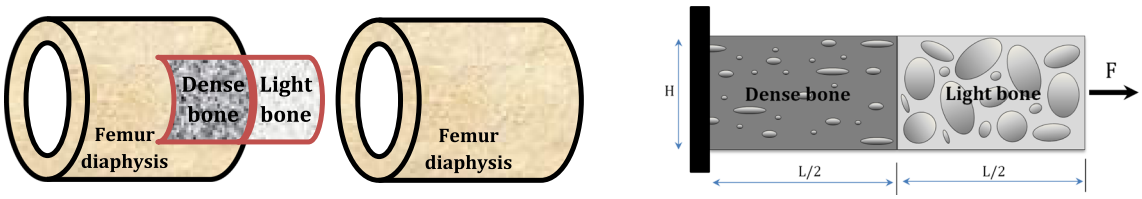

Fig. 1 Model definition—**a** extraction from real bone conditions, and **b** definition of the model geometry and boundary conditions

Table 1 Theoretical model-dependent parameters

α_{mech}	Weighting coefficient for the mechanical stimulus	0.6
α_{O2}	Weighting coefficient for the oxygen molecular stimulus	4
α_{CHO}	Weighting coefficient for the glucose molecular stimulus	4
α_{ob}	Weighting coefficient for the osteoblast cellular stimulus	2
α_{oc}	Weighting coefficient for the osteoclast cellular stimulus	2

longitudinal axis of a femur diaphysis is considered as presented in Fig. 1a. While the dense cortical bone remains on the left and right side of the diaphysis, the empty space in between needs to be filled. In the current work, we assume that it is filled with a bone scaffold (low density, no biology). Once the initial conditions fixed and mechanical load applied, the biological constituents of the dense bone will transfer from the original cortical bone to the reconstruction zone. Hence, on the one side, we have the existing "dense" cortical bone, and on the other side the critical default needing reconstruction starting with the "bone scaffold" or "light" bone. The model focuses on the mechanobiological interplay and migration phenomena occurring through the interface for the bone reconstruction to occur (hence being of the order of centimetres at a macroscopic scale). A 1-dimensional problem on the one hand would not be adequate to observe the complex phenomena at play. On the other hand, a 3-dimensional model would require extensive numerical resources without bringing extensive additional understanding to the problem at hand. Hence, a two-dimensional study was developed in order to highlight the studied couplings.

These mechanobiological couplings are developed through the analytical framework described in Sect. 2.1 and applied on a two-dimensional cantilever beam of length $L = 5\,\text{cm}$ and height $H = 1.6\,\text{cm}$ under simple tension corresponding to a standard person's body weight $F = 750\,\text{N}$ (see Fig. 1b).

In addition, as presented in equation (1), the α_i parameters are theoretical model dependent being different for each patient (as the importance of each stimulus can vary from one patient to another) as well as their respective ratio. As the current work aims at presenting mainly the existing couplings between the mechanical stimulus and cell activation, we define these in Table 1 as initial conditions that will need to be optimized in future works.

Hence, the proposed problem corresponds to an average standard bone size sample for which we are more specifically interested in what occurs at the mid-length interface. In the following, we suppose that no internal body forces develop (no body weight) so that $f_v = 0$ in the equilibrium equation.

The initial mechanical conditions of the problem were defined from the literature [57] and are such that, the left half side of the beam is filled with higher bone density ($\rho_{b,ini}^{left} = 0.6$), whereas the right half side of the beam is constituted by lighter bone density ($\rho_{b,ini}^{right} = 0.1$) and is assumed to represent a bone area to be reconstructed. As the applied external mechanical force corresponds to standard body weight, when applied within the hypothesis of zero flux on the boundary of the problem, migration of cells and nutriments occurs from left (dense bone region) to right (light bone region). The bone density thence increases in both regions with a minimum value of $0 (\rho_{\text{bone}}^{\min} = \rho_{\min} = 0\%)$ and a maximum value of $1 (\rho_{\text{bone}}^{\max} = \rho_{\max} = 100\%)$.

Complementarily, initial biological concentrations are defined for a given specific scenario to study and can be adjusted depending on patient characteristics. They are given in Table 2.

Finally, the main input biological parameters highlighting the mechanobiological couplings of the model are listed in Table 3. Of these nine independent parameters, the first three D_i are geometrical parameter representing sensibility threshold distance above which each stimulus becomes negligible. They can be used as tuneable optimization to confirm or infirm results obtained to quantify the stimulus sensitivity threshold in mechanobiological tests. Out of the six remaining parameters, five only need to be tuned with coupled

Table 2 Initial patient-dependent biological concentrations

c_{ob}	Initial concentration of osteoblasts on the left of the beam	0.1
c_{oc}	Initial concentration of osteoclasts on the left of the beam	0.05
c_{O2}	Initial concentration of oxygen on the left of the beam	0.2
c_{CHO}	Initial concentration of glucose on the left of the beam	0.1

Table 3 Main parameters of the model

Parameter	Description	Value
D_{mech}	Characteristic distance accounting for the dependent size effect of the mechanical load	3 mm
$D_{O2,CHO}$	Characteristic distances of molecular activation thresholds	3 mm
$D_{ob,oc}$	Characteristic distances of the osteoblasts and osteoclasts activation thresholds	3 mm
ϕ	Diffusion tensor scalar	10
k_{oc}	Osteoclasts proliferation rate	0
k_{ob}	Osteoblasts proliferation rate	3
β_{ob}	Osteoclasts differentiation rate	15
s_b	Bone synthesis rate	1
r_b	Bone resorption rate	4

experiments in order to validate the model predictions. The 1 to 4 ratio between the bone synthesis and resorption has already been quantified experimentally in [58]. The choice of no osteoclast proliferation rate is explained by the fact that, in bone remodelling, osteoclasts are present at the beginning in order to "clean" the place before the osteoblasts arrive and start reconstructing the bone. As we are here in a reconstruction process only, we skip the first stage and osteoclasts being present are only differentiated or degraded without renewal leaving the place for the bone reconstruction to occur. Hence, there remain only four biological parameters needing to be experimentally adjusted; the diffusion tensor, the osteoblasts proliferation, the osteoclasts differentiation, and either, the bone synthesis or the bone resorption rate (these are partially known in the literature for specific cases).

Also, an artificial time was defined in the analysis corresponding to the average 3 months bone reconstruction while ensuring consistent results.

3 Results and discussion

The results of the proposed model are presented here in two parts. The first part shows the distribution of the defined parameters through the geometry at different times of the analysis. The strain distribution and associated mechanical stimulus are presented in Fig. 2. Figure 3 shows the evolution of the osteoclasts and osteoblasts concentration, and associated cellular stimulus over time. Figure 4 shows the oxygen and glucose concentrations and corresponding stimulus. Finally, Fig. 5 presents the total stimulus and bone density evolutions. In the second part, evolutions are presented at four different locations (see Fig. 6) on the geometry for the concentrations and corresponding stimulus in Figs. 7, 8, and 9.

As expected from the material mechanical parameters, the developed strain (see Fig. 2) is small on the left side (with a density $\rho_b = 0.6$) with a sharp gradient at the interface and increasing on the right side due to low bone density ($\rho_b = 0.1$). The mechanical stimulus being an exponentially decreasing integral of the elastic strain energy density shows a peak value at the interface between dense bone and light bone. As the strain distribution changes (due to the bone reconstruction from left to right and change in the mechanical properties), the mechanical stimulus follows in time the reconstruction interface between dense and light bone. We also observe, from the initial and final bone density distribution, that the strain and mechanical stimulus are more important on the border of the geometry at the beginning and end of analysis, but not in the middle as bone density is reconstructed first in the central part of the beam, which decreases the developed elastic strain energy.

In Fig. 3, concentrations evolve with nonlinear distributions. A clear diffusion from the left to the right of the beam is observed leading to an increase of them on the right side of the beam. The initial density distributions show a dome shape stimulus on the left (due to the exponentially decreasing integral) and zero stimulus on the right side as no cells are present. As the analysis evolves and bone density changes (see Fig. 5), a non-constant distribution is observed. The cell motility shows its dependence on the developed strain due to

Arbitrary time	Strain	Mechanical stimulus
0	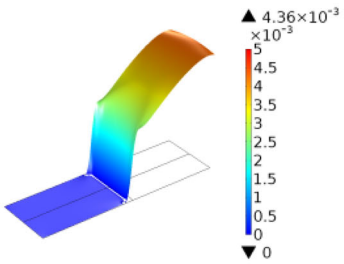	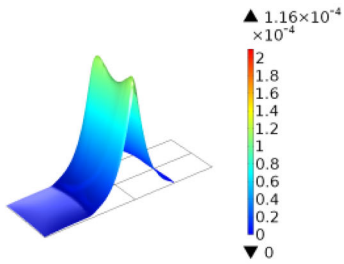
0.2	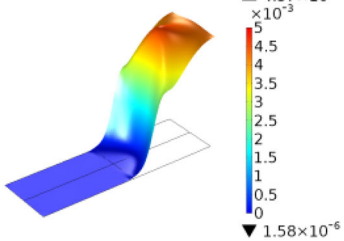	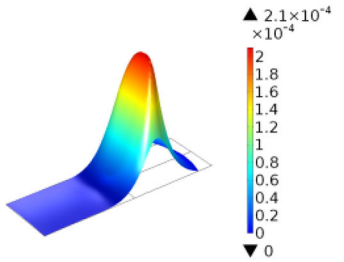
0.4	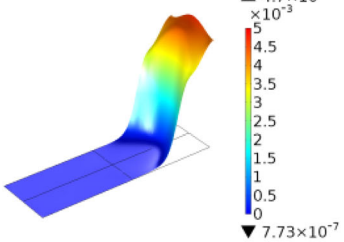	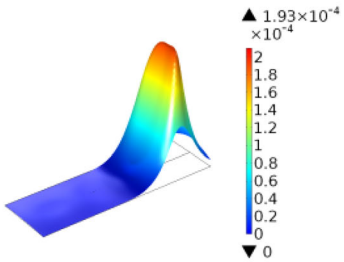
0.7	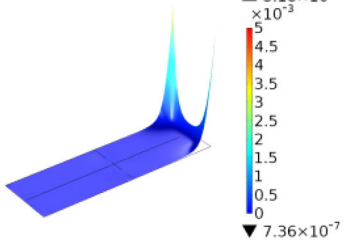	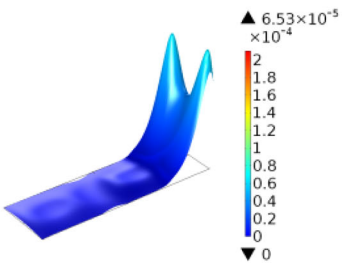
1	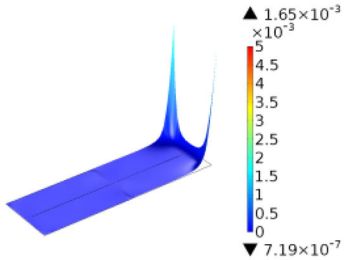	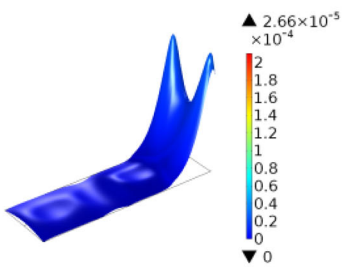

Fig. 2 Evolution of the strain distribution and associated mechanical stimulus over time

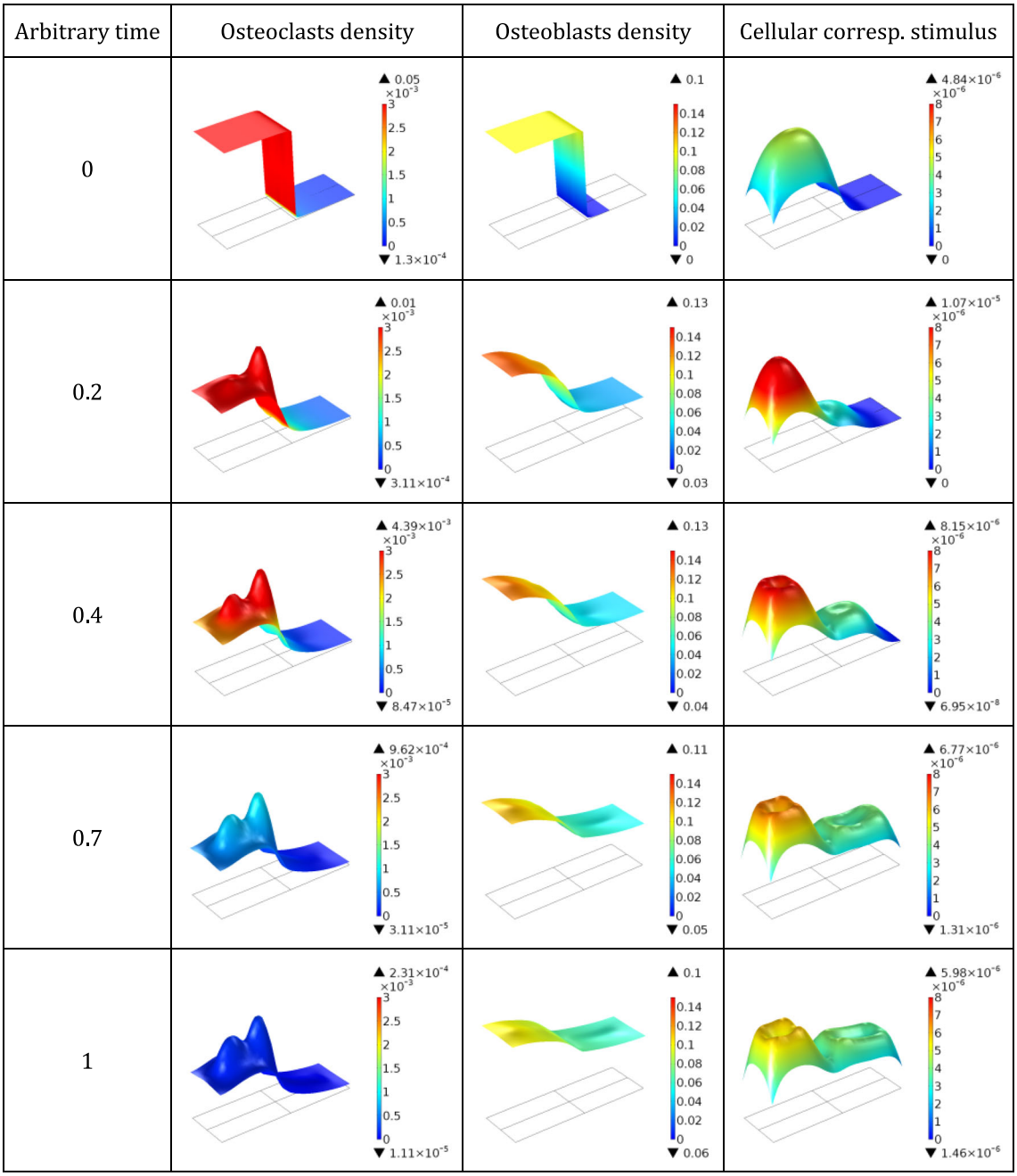

Fig. 3 Evolution of the osteoclasts and osteoblasts concentration, and associated cellular stimulus over time

the mechanical properties and bone density dependence. Hence, faster cell kinetics is observed in low bone density regions. Also, since only osteoclasts differentiation to osteoblasts is considered here by hypothesis, we can observe its continuous decrease over time. On the contrary, osteoblasts are developing both from the osteoclasts differentiation and their own proliferation, which is observed through an increase and a migration on each side of the beam. For the developed cellular stimulus, it is a combination of the positive contribution coming from osteoblasts and the negative contribution coming from osteoclasts, together with a dependence on the bone density distribution. We can observe clearly this effect on the central part of both sides of the beam where the cellular stimulus is developed with lower positive values in the centres and higher ones in between the centres and the borders. Of course, this cellular stimulus distribution is directly dependent on the defined hypotheses of the theoretical models and will change accordingly to other hypotheses.

The glucose concentration and the corresponding molecular stimulus are presented in Fig. 4. Note that only glucose is presented here but oxygen follows exactly the same kinetics and interpretations, only with different intensities (Initial oxygen concentration is 0.2 and initial glucose concentration is 0.1). We observe that concentrations are diffusing quicker than osteoblasts and osteoclasts as their final distribution through the length of the beam is constant at the end of the analysis ($c_{OHO} = 0.05$), which is not the case for osteoblasts ($0.08 < c_{ob} < 0.1$). The initial molecular stimulus distribution follows the same trend as for the cellular stimulus. However, the migration of oxygen and glucose follows a simple diffusion equation that does not depend on the developed strain (as compared to the cellular migration). Hence, the distribution of oxygen and glucose with time does not suffer nonlinear geometrical distribution, but only through the length of the beam as a function of the diffusion process. On the contrary, the molecular stimulus follows the same rules as detailed above which explains its distribution.

The strain dependence of the cell and molecular kinetics is, in this proposed model, defined without a priori knowledge and would require to be validated with experimental results. Also, strain is probably not the only driving parameter for the cellular and molecular kinetics. Other biological factors may influence them and need to be identified, quantified and integrated, in order to obtain a better prediction of their influence into the bone density kinetics process. Finally, the integration of such effects in a continuum mechanics theoretical model also requires the validation of both the thermodynamic equilibrium together with biological equilibrium in order to fulfil an adequate living system.

The calculated global stimulus and bone density evolution over time are presented in Fig. 5. It represents the couplings between the mechanical stimulus (J/m^3) and biological effects (non-dimensional). The total maximum stimulus shows a peak value of 8.61 J/m^3 at the beginning of the analysis due to the sharp gradient of bone density located at the beam mid-length. As bone reconstruction occurs through the beam, this intensity decreases progressively. This maximum peak (due to the mechanical energy developed) propagates from left to right to finally nearly vanish due to the bone density increase. This kinetics is directly dependent on the one of bone density. The cellular and molecular stimuli having smaller intensities are hardly visible although playing an important role. This role is clearly visible on the left side of the beam in the bone density evolution. Bone density increases on the left side under mostly equivalent contributions from all three stimuli (mechanical, cellular, and molecular). This is due to its higher density and the presence of cells and molecular concentrations at the start of the analysis on the left side, whereas they are not present on the other side.

The total stimulus is maximum at the location of the highest strain gradient but is also nonzero at other places due to the contributions of the cellular and molecular effects. The mechanical stimulus shows the highest impact, in terms of time-dependent kinetics, on the bone reconstruction. This does not mean that long term reconstruction would be better or worse only as a function of non-mechanical stimulus, but needs to be quantified and validated. From the initial bone densities distributions (0.6 on the left and 0.1 on the right), the bone kinetics is mainly triggered by the mechanical stimulus on the right side due to weak bone density with no biology, but mainly the biological stimulus on the left side due to higher bone density and the presence of biology.

The interpretation of the results shown in Figs. 4 and 5 enable comparing the predicted bone density evolution with theoretical numerical models based on strain energy density only. As with a structural optimization problem, the bone density is only dependent on the developed strain energy within the structure. The equilibrium between the developed mechanical energy and biology is based on the thresholds under which we have bone degradation and above which we have bone reconstruction. It is always possible to obtain a similar bone density evolution for the two different approaches for a given constant bone density at one place. However, as both the biological and mechanical stimulus have differently defined kinetics as a function of the bone density (the mechanical stimulus is directly dependent on the developed mechanical strain as the biological stimulus is mainly dependent on the presence or not of the biological contributions), when a bone density gradient exists within the structure, the two models cannot provide the same answer. Hence, it feels awkward to propose a structural optimization without accounting for the biological contributions at their respective places within the structure.

Once bone density has mostly reconstructed (reaching homeostasis), equilibrium between mechanical and biological stimuli is reached. Biological contributions become then predominant over longer periods of time. Although the mechanical stimulus plays a determinant role in the bone density kinetics, it is also highly dependent on the biological contributions and coupled with the bone density. High bone density leads to small strains (and therefore small mechanical stimulus), whereas low bone density leads to high strains and large mechanical stimulus. However, it is not possible to impose a high mechanical load on weak bone density to obtain faster bone reconstruction due to possible fracture of the structure. This is where the biological

Arbitrary time	Glucose concentration	Glucose corresp. stimulus
0	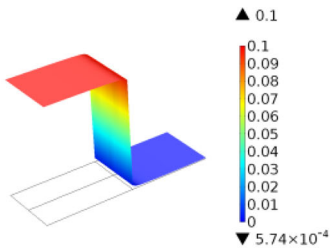	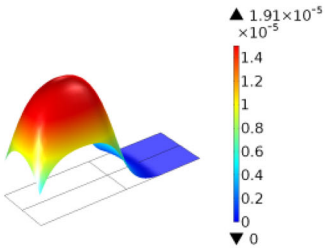
0.2	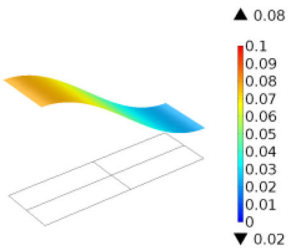	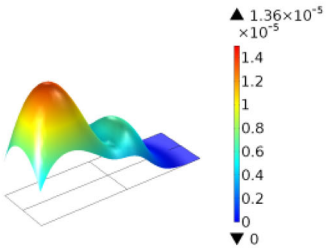
0.4	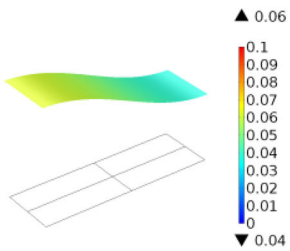	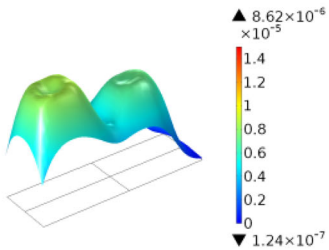
0.7	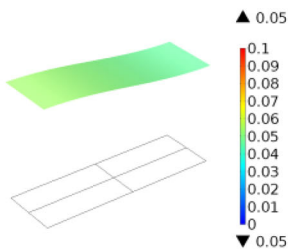	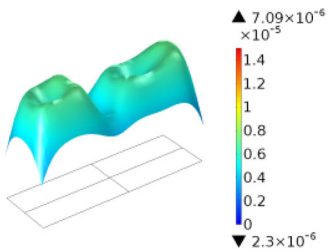
1	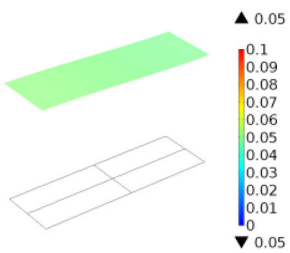	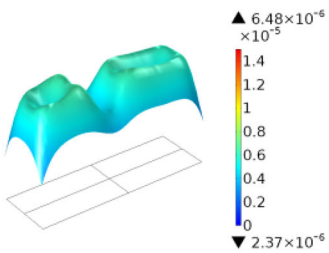

Fig. 4 Evolution of the oxygen and glucose concentration, and associated molecular stimulus over time

Arbitrary time	Total stimulus	Bone density
0	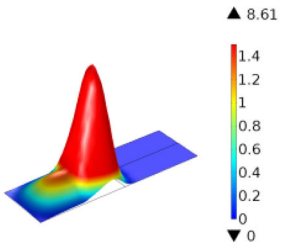	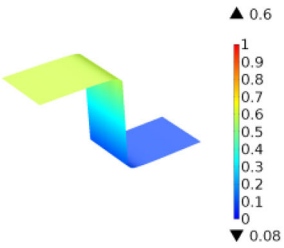
0.2	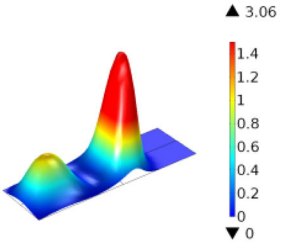	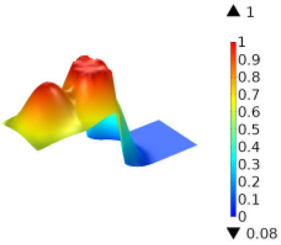
0.4	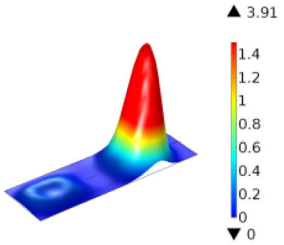	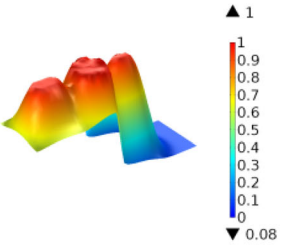
0.7	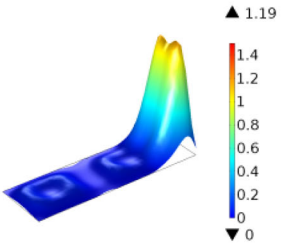	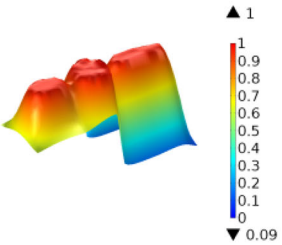
1	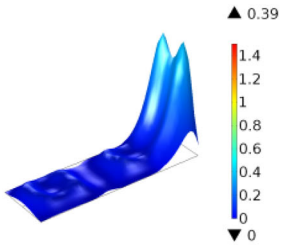	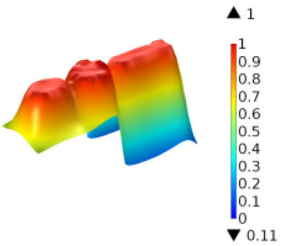

Fig. 5 Evolution of the total stimulus (mechanical, cellular and molecular) and the bone density over time

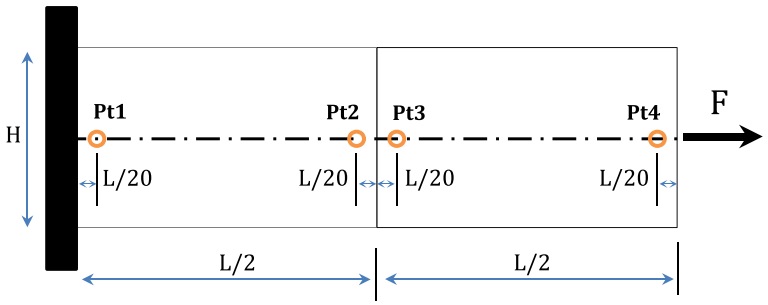

Fig. 6 Definition of measurement point locations for Figs. 7, 8, and 9

contributions play a critical role and certainly impact strongly the time evolutions. A possible equilibrium may take place between mechanical and biological stimuli for this particular reason but needs to be quantified. Hence, the modelling of bone reconstruction through weak bone density or bone substitutes only using strain energy density lacks important contribution from the biological contributions.

We present additional results of this work at four locations (Pt1 to Pt4) through the length of the beam as presented on Fig. 6.

Figure 7 shows the cellular and molecular concentrations kinetics as a function of time. For osteoclasts concentration, as there is no differentiation nor creation by hypothesis, their density is only vanishing towards zero. For the osteoblasts, on the contrary, they are supposed both differentiated from osteoclasts and multiplied. Hence, depending on the positions, we observe on the left side a density increase from 0.1, a decrease/increase at the dense/light bone interface respectively, and an increase on the right side due to cell migration. We observe that the cell concentrations (osteoblasts and osteoclasts) tend to reach equilibrium with time in the whole geometry. It seems that this effect is a combination of both the molecular distribution equilibrium and constant bone density reconstruction in the beam. The evolution kinetics is nonlinear as a function of the developed strains (depending on the bone density) inside the beam.

For the molecular distribution, equilibrium is reached faster and only depends on the initial parameters. Equilibrium is reached for the average of the initial concentration defined at 0.1 and 0.2 at the beginning of the analysis due to the diffusion processes defined.

Figure 8 presents the evolutions of each of the four stimuli (mechanical, cellular, oxygen and glucose) as a function of time for each of the four measurement points. For the mechanical stimulus, we observe that at the left extremity, almost no mechanical stimulus is developed at any time due to the existing bone density far away from the strain gradient. However, the mechanical stimulus develops mainly at the interface at the beginning, then later on at the right extremity as the bone has reconstructed. We also observe that the mechanical stimulus shows an equivalent peak magnitude as the bone reconstruction goes on since the mechanical properties are supposed to be homogeneous and isotropic. This is also due to the fact that cellular and molecular distributions diffuse in a homogenized way through the geometry.

The cellular stimulus, on the contrary to the mechanical stimulus shows a high intensity on the left side at the beginning since concentration and proliferation are the highest. For the other three locations, diffusion is highest at the interface, hence showing lower stimulus intensity, and with diffusion time through the beam length shows an increase later on, on the right side. In the same way as for the cellular concentration, the stimulus tends towards the equilibrium at the end of analysis when the cells, mechanics and molecular distribution average with constant bone density.

For the molecular stimuli, oxygen and glucose both show exactly the same kinetics. This is due to the identical kinetics hypothesized with only different initial concentrations. The trends are similar to the one of the cellular stimulus, only the diffusion equation is different. Hence similar interpretation of results can be made.

Finally, Fig. 9 shows the evolution of bone density at the four location points as a function of time. It follows the interpretations made for the different developed stimuli. At the left location, a small mechanical stimulus is developed, but the biological stimuli remain, and hence bone density is increasing with slower kinetics. At the dense/light bone interface, high strain gradient is generated leading to a fast bone reconstruction. Nevertheless, before the mid-time analysis ($t = 0.4$) bone density on the left side of the interface has reached a level decreasing largely the mechanical stimulus, which leads to a smaller bone density evolutions with mostly

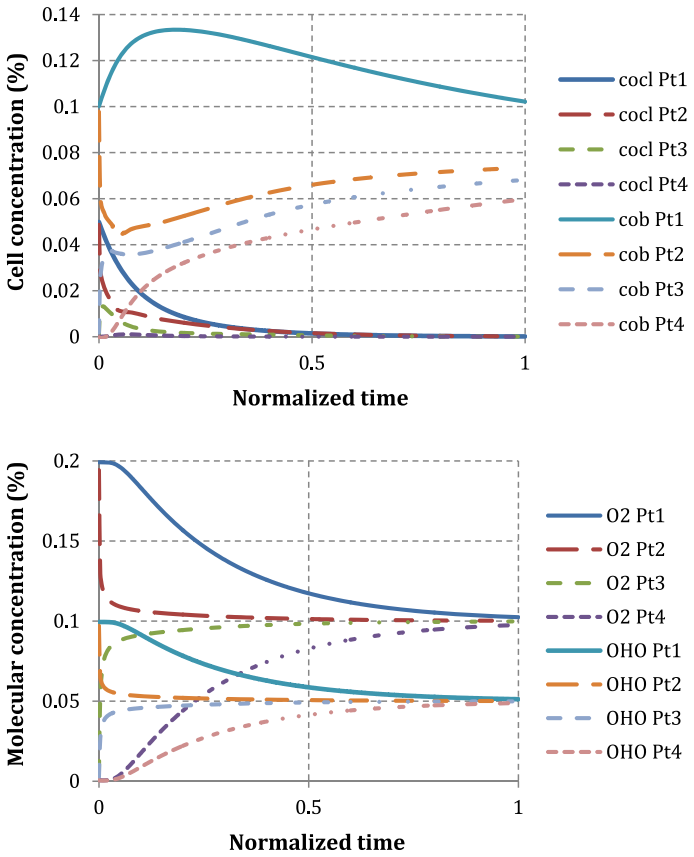

Fig. 7 Cellular and molecular kinetics as a function of time for the four measurement locations

the biological stimuli having an effect. Similar observation is made on the right side of the beam, once the mechanical stimulus has reconstructed a large part of the bone density.

Although the different accounted stimuli in this work are always positive (it is supposed that we are in a positive evolutionary situation with applied external mechanical load that leads the total stimulus to be outside the so-called lazy zone), the theoretical framework developed is designed to account for situation where couplings between no force with existing biological stimulus or applied mechanical forces with near zero biological stimulus can be done. However, in order to be able to account for these different effects and be able to quantify them, it is required to be able to experimentally measure the initial thresholds and evolutionary parameters of the model, but also the time-dependent variables such as cell apoptosis without nutriments.

4 Conclusion

We presented a coupled multiphysics theoretical numerical model to compute bone reconstruction using a continuum mechanics approach of the coupled mechanobiological stimulus. The specific mechanical (through external forces) and biological (through cellular and molecular functions) phenomena are integrated within the same stimulus and show their respective contributions and couplings on the kinetics of bone reconstruction. More precisely, the mechanical effects showed to be more important at the beginning of the reconstruction when high strain energy is developed with lower bone density. Then, biological effects (through cellular activation, migration, and proliferation/differenciation, being supported by molecular intake) take over since the strain energy is decreased and longer time bone reconstruction develops. These couplings are intimately correlated with the bone density distribution but also depend highly on the defined boundary conditions of the problem together with the input parameters of the model. Detailed analyses are necessary to identify more precisely these effects and quantify the respective importance of each parameter with experimental validations. This will

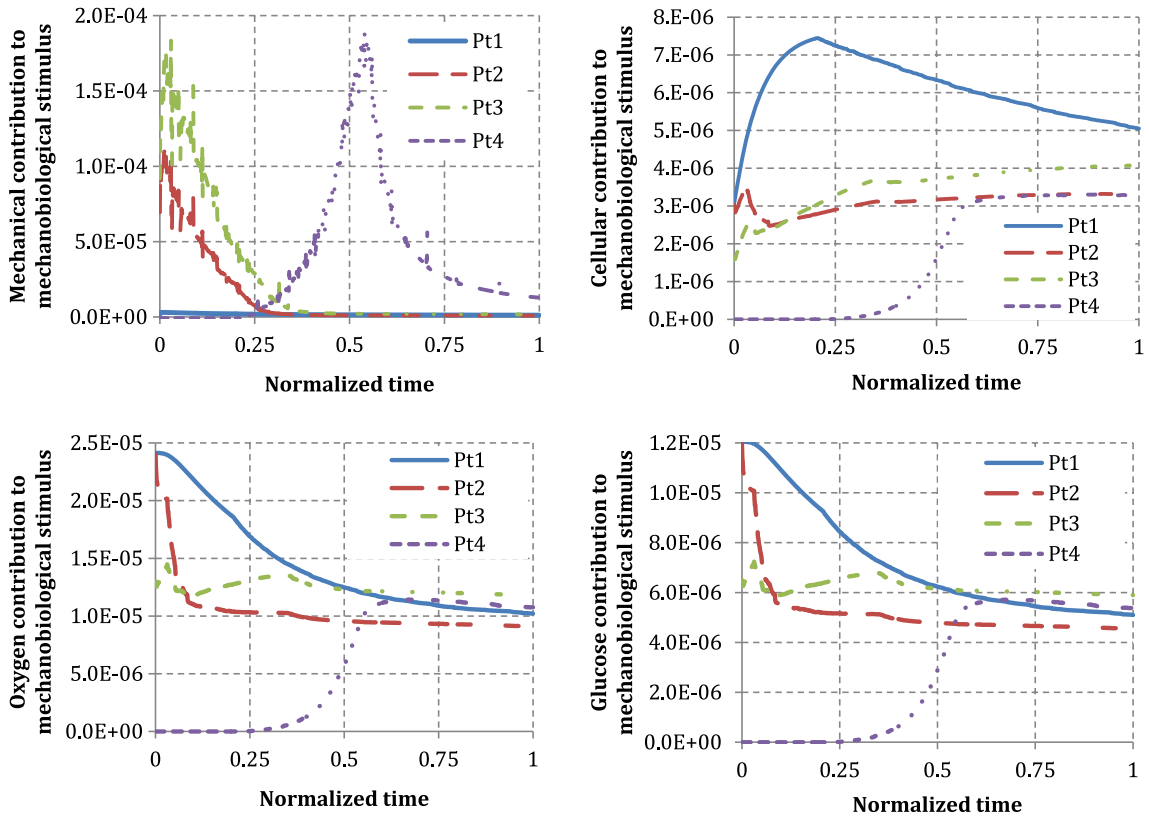

Fig. 8 Mechanical, cellular and molecular contributions to total stimulus for each locations

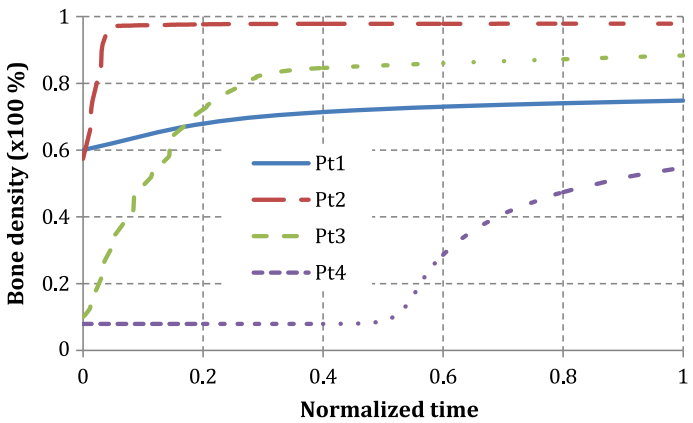

Fig. 9 Bone density evolution as a function of time for each four locations

help in better understanding of the complex problems of bone reconstruction that needs to be integrated with the mechanobiological bone environment and healing processes through vascular growth and nutrient supply for better representation of real life situation.

References

1. Frost, H.: Bone "mass" and the "mechanostat": a proposal. J. Anat. Rec. **219**, 1–9 (1987)
2. Cowin, S.C.: Wolff's law of trabecular architecture at remodeling equilibrium. J. Biomed. Eng. **108**(1), 83–88 (1986)
3. Beaupré, G.S., Orr, T.E., Carter, D.R.: An approach for time-dependent bone modeling and remodeling–application: a preliminary remodeling simulation. J. Orth. Res. **8**(5), 662–670 (1990)

4. Turner, C.H.: Three rules for bone adaptation to mechanical stimuli. Bone **23**(5), 399–407 (1998)
5. Pivonka, P., Zimak, J., Smith, D.W., Gardiner, B.S., Dunstan, C.R., Sims, N.A.: Model structure and control of bone remodeling: a theoretical study. Bone **43**(2), 249–263 (2008)
6. Pivonka, P., Komarova, S.V.: Mathematical modeling in bone biology: from intracellular signaling to tissue mechanics. Bone **47**(2), 181–189 (2010)
7. Lekszycki, T.: Modeling of bone adaptation based on an optimal response hypothesis. Meccanica **37**, 343–354 (2002)
8. Madeo, A., Lekszycki, T., Dell'Isola, F.: A continuum model for the bio-mechanical interactions between living tissue and bio-resorbable graft after bone reconstructive surgery. C.R. Mécanique **339**, 625–640 (2011)
9. Madeo, A., George, D., Lekszycki, T., Nierenberger, M., Rémond, Y.: A second gradient continuum model accounting for some effects of micro-structure on reconstructed bone remodeling. C.R. Mécanique **340**, 575–589 (2012)
10. Lekszycki, T., Dell'Isola, F.: A mixture model with evolving mass densities for describing synthesis and resorption phenomena in bones reconstructed with bio-resorbable materials. ZAMM **92**, 426–444 (2012)
11. Madeo, A., George, D., Rémond, Y.: Second-gradient models accounting for some effects of microstructure on remodelling of bones reconstructed with bioresorbable materials. Comp. Meth. Biomech. Biomed. Eng. **16**(sup1), 260–261 (2013)
12. Andreaus, U., Giorgio, I., Lekszycki, T.: A 2-D continuum model of a mixture of bone tissue and bio-resorbable material for simulating mass density redistribution under load slowly variable in time. ZAMM **94**, 978–1000 (2014)
13. dell'Isola, F., Andreaus, U., Placidi, L.: At the origins and in the vanguard of peridynamics, non-local and higher-gradient continuum mechanics: An underestimated and still topical contribution of Gabrio Piola. Math. Mech. Sol **20**(8), 887–928 (2015)
14. Misra, A., Poorsolhjouy, P.: Identification of higher-order elastic constants for grain assemblies based upon granular micromechanics. Math. Mech. Comp. Syst. **3**(3), 285–308 (2015)
15. Ganghoffer, J.F.: Spatial and material stress tensors in continuum mechanics of growing solid bodies. Math. Mech. Comp. Syst. **3**(4), 341–363 (2015)
16. Placidi, L., Andreaus, U., Della Corte, A., Lekszycki, T.: Gedanken experiments for the determination of two-dimensional linear second gradient elasticity coefficients. Zeit. Ang. Math. Phys. **66**(6), 3699–3725 (2015)
17. George, D., Spingarn, C., Madeo, A., Rémond, Y.: Effects of mechanical loading conditions on 3D bone reconstruction: a theoretical numerical study for application to Maxillo-facial surgery. In: Proceedings of the 9th European Solid Mechanics Conference, Madrid, Spain (2015)
18. Giorgio, I., Andreaus, U., Scerrato, D., Dell'Isola, F., et al.: A visco-poroelastic model of functional adaptation in bones reconstructed with bio-resorbable materials. Biomech. Model Mechanobiol. **15**, 1325–1343 (2016)
19. Scala, I., Spingarn, C., Rémond, Y., Madeo, A., George, D.: Mechanically-driven bone remodeling simulation: application to LIPUS treated rat calvarial defects. Math. Mech. Sol. **22**(10), 1976–1988 (2016)
20. Spingarn, C., Rémond, Y., George, D.: Techniques de changement d'échelles pour la modélisation de tissus biologiques, Conf. MECAMAT, Mécanique pour le vivant, Aussois, France (2016)
21. Abali, B.E., Müller, W.H., dell'Isola, F.: Theory and computation of higher gradient elasticity theories based on action principles. Arch. App. Mech. **87**(9), 1495–1510 (2017)
22. Turco, E.: Tools for the numerical solution of inverse problems in structural mechanics: review and research perspectives. Eur. J. Env. Civ. Eng. **21**(5), 509–554 (2017)
23. dell'Isola, F., Della Corte, A., Giorgio, I.: Higher gradient continua: the legacy of Piola, Mindlin, Sedov and Toupin and some future research perspectives. Math. Mech. Sol. **22**(4), 852–872 (2017)
24. Templet, G.J., Steigmann, D.J.: On the theory of diffusion and swelling in finitely deforming elastomers. Math. Mech. Comp. Syst. **1**(1), 105–128 (2013)
25. George, D., Rémond, Y.: Multiscale mechanobiology of human tissue: experiment and modelling. In: 6th International Symposium Europe China, Molecular, cellular and tissue engineering, and clinical applications, Nancy, France (2016)
26. George, D., Spingarn, C., Dissaux, C., Rémond, Y.: Understanding bone mechanobiology to predict bone reconstruction kinetics: application to maxillo-facial surgery, XII Rencontres du Vietnam, Mechanobiology, from molecules to tissue, Quy Nhon, Vietnam (2016)
27. Spingarn, C., Wagner, D., Rémond, Y., George, D.: Multiphysics of bone remodeling: a 2D mesoscale activation simulation. Bio-Med. Mat. Eng. **28**(s1), S153–S158 (2017)
28. Cuomo, M.: Forms of the dissipation function for a class of viscoplastic models. Math. Mech. Comp. Syst. **5**(3–4), 217–237 (2017)
29. Giorgio, I., Andreaus, U., Dell'Isola, F., Lekszycki, T.: Viscous second gradient porous materials for bones reconstructed with bio-resorbable grafts. Ext. Mech. Let. **13**, 141–147 (2017)
30. George, D., Spingarn, C., Dissaux, C., Nierenberger, M., Rahman, R.A., Rémond, Y.: Examples of multiscale and multiphysics numerical modeling of biological tissues. Bio-Med. Mat. Eng. **28**(S1), S15–S27 (2017)
31. Lemaire, T., Capiez-Lernout, E., Kaiser, J., Naili, S., Sansalone, V.: What is the importance of multiphysical phenomena in bone remodelling signals expression? A multiscale perspective. J. Mech. Behav. Biom. Mat. **4**(6), 909–920 (2011)
32. Sansalone, V., Gagliardi, D., Descelier, C., Haiat, G., Naili, S.: On the uncertainty propagation in multiscale modeling of cortical bone elasticity. Comp. Meth. Biom. Biomed. Eng. **18**, 2054–2055 (2015)
33. Bednarczyk, E., Lekszycki, E.: A novel mathematical model for growth of capillaries and nutrient supply with application to prediction of osteophyte onset. ZAMP **67**, 94 (2016)
34. Lu, Y., Lekszycki, T.: A novel coupled system of non-local integro-differential equations modelling Young's modulus evolution, nutrients' supply and consumption during bone fracture healing. ZAMP **67**, 111 (2016)
35. Moya, A., Paquet, J., Deschepper, M., et al.: Human mesenchymal stem cell failure to adapt to glucose shortage and rapidly use intracellular energy reserves through glycolysis explains poor cell survival after implantation. Stem Cells **36**, 363–376 (2018). https://doi.org/10.1002/stem.2763
36. Paquet, J., Deschepper, M., Moya, A., et al.: Oxygen tension regulates human mesenchymal stem cell paracrine functions. Stem Cells Trans. Med. **4**(7), 809–821 (2015)

37. Deschepper, M., Oudina, K., David, B., Myrtil, V., Collet, C., Bensidhoum, M., Logeart-Avramoglou, D., Petite, H.: Survival and function of mesenchymal stem cells (MSCs) depend on glucose to overcome exposure to long-term, severe and continuous hypoxia. J. Cell. Mol. Med. **15**(7), 1505–14 (2011)
38. Farrel, M.J., Shin, J.I., Smith, L.J., Mauck, R.L.: Functional consequences of glucose and oxygen deprivation on engineered mesenchymal stem cell-based cartilage constructs. Osteoarthr. Cartil. **23**(1), 134–42 (2015)
39. Cisewski, S.E., Zhang, L., Kuo, J., Wright, G.J., Wu, Y., Kem, M.J., Yao, H.: The effects of oxygen level and glucose concentration on the metabolism of porcine TMJ disc cells. Osteoarthr. Cartil. **23**(10), 1790–6 (2015)
40. Wagner, D., Bolender, Y., Rémond, Y., George, D.: Mechanical equilibrium of forces and moments applied on orthodontic brackets of a dental arch : correlation with litterature data on two and three adjacent teeth. Bio-Med. Mat. Eng. **28**, S169–S177 (2017)
41. Martin, M., Lemaire, T., Haiat, G., Pivonka, P., Sansalone, V.: A thermodynamically consistent model of bone rotary remodeling: a 2D study. Comp. Meth. Biomech. Biomed. Eng. **20**(S1), 127–128 (2017)
42. Rémond, Y., Ahzi, S., Baniassadi, M., Garmestani, M.: Applied RVE reconstruction and homogenization of heterogeneous materials, Ed. Wiley-ISTE ISBN: 978-1-84821-901-4 (2016)
43. Burr, D.B., Allen, M.R.: Basic and Applied Bone Biology, pp. 85–86. Academic Press, Cambridge (2013)
44. Lemaire, T., Naïli, S., Rémond, A.: Multiscale analysis of the coupled effects governing the movement of interstitial fluid in cortical bone. Biomech. Mod. Mech. **5**(1), 39–52 (2006)
45. Lemaire, T., Naili, S., Sansalone, V.: Multiphysical modelling of fluid transport through osto-articular media. An. Ac. Bras. Ciências **82**(1), 127–144 (2010)
46. Lemaire, T., Kaiser, J., Naili, S., Sansalone, V.: Three-scale multiphysics modeling of transport phenomena within cortical bone. Math. Prob. Eng. 398970 (2015)
47. Allena, R., Maini, P.K.: Reaction–diffusion finite element model of lateral line primordium migration to explore cell leadership. Bull. Math. Biol. **76**(12), 3028–3050 (2014)
48. Schmitt, M., Allena, R., Schouman, T., Frasca, S., Collombet, J.M., Holy, X., Rouch, P.: Diffusion model to describe osteogenesis within a porous titanium scaffold. Comp. Meth. Biomech. Biomed. Eng. **19**(2), 171–179 (2015)
49. Frame, J., Rohan, P.Y., Corté, L., Allena, R.: A mechano-biological model of mulit-tissue evolution in bone, Cont. Mech. Thermo. 1–13 (2017) (in press). https://doi.org/10.1007/s00161-017-0611-9
50. George, D., Allena, R., Rémond, Y.: Mechanobiological stimuli for bone remodeling: mechanical energy, cell nutriments and mobility. Comp. Meth. Biomech. Biomed. Eng. **20**, S91–S92 (2017)
51. Hambli, R., Rieger, R.: Physiologically based mathematical model of transduction of mechanobiological signals by osteocytes. Biomech. Model Mechanobiol. **11**(1–2), 83–93 (2012)
52. Hambli, R., Kourta, A.: A theory for internal bone remodeling based on interstitial fluid velocity stimulus function. App. Math. Mod. **39**(12), 3525–3534 (2015)
53. Currey, J.D.: The effect of porosity and mineral content on the Young's modulus of elasticity of compact bone. J. Biomech. **21**(2), 131–139 (1988)
54. Rho, J.Y., Ho Ba Tho, M.C., Ashman, R.B.: Relations of mechanical properties to density and CT numbers in human bone. Med. Eng. Phys. **17**(5), 347–355 (1995)
55. Gibson, L.J.: The mechanical behaviour of cancellous bone. J. Biomech. **18**(5), 317–328 (1985)
56. Lai, Y.-S., Chen, W.-C., Huang, C.-H., Cheng, C.-K., Chan, K.-K., Chang, T.-K.: The effect of graft strength on knee laxity and graft in-situ forces after posterior cruciate ligament reconstruction. PLoS One **10**(5), e0127293 (2015)
57. Renders, G.A.P., Mulder, L., Van Ruijven, L.J., Van Eijden, T.M.G.J.: Porosity of human mandibular condylar bone. J. Anat. **210**(3), 239–248 (2007)
58. Burr, D.B., Allen, M.R.: Basic and Applied Bone Biology. Elsevier Inc, Amsterdam (2013)